

# Selection of In Silico Drug Screening Results for G-Protein-Coupled Receptors by Using Universal Active Probes

Mitsuhiro Wada,<sup>†,‡</sup> Eiji Kanamori,<sup>†,§</sup> Haruki Nakamura,<sup>⊥</sup> and Yoshifumi Fukunishi<sup>\*,||</sup>

<sup>†</sup>Japan Biological Informatics Consortium (JBIC), 2-3-26, Aomi, Koto-ku, Tokyo 135-0064, Japan

<sup>‡</sup>Biochemical Information Project, Fujitsu Limited, 1-9-3 Nakase, Mihama-ku, Chiba 261-8588, Japan

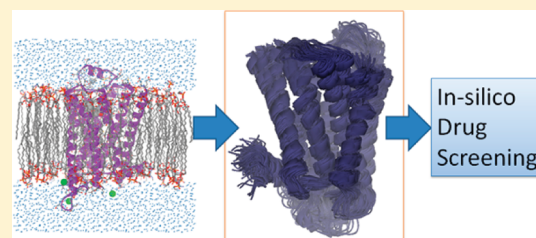
<sup>§</sup>Hitachi Solutions, Ltd., 1-1-43, Suehiro-cho, Tsurumi-Ku, Yokohama, Kanagawa 230-0045, Japan

<sup>⊥</sup>Institute for Protein Research, Osaka University, 3-2 Yamadaoka, Suita, Osaka 565-0871, Japan

<sup>||</sup>Biomedical Information Research Center (BIRC), National Institute of Advanced Industrial Science and Technology (AIST), 2-3-26, Aomi, Koto-ku, Tokyo 135-0064, Japan

**S** Supporting Information

**ABSTRACT:** We developed a new protocol for in silico drug screening for G-protein-coupled receptors (GPCRs) using a set of “universal active probes” (UAPs) with an ensemble docking procedure. UAPs are drug-like compounds, which are actual active compounds of a variety of known proteins. The current targets were nine human GPCRs whose three-dimensional (3D) structures are unknown, plus three GPCRs, namely  $\beta_2$ -adrenergic receptor (ADRB2),  $A_{2A}$  adenosine receptor ( $A_{2A}$ ), and dopamine D3 receptor ( $D_3$ ), whose 3D structures are known. Homology-based models of the GPCRs were constructed based on the crystal structures with careful sequence inspection. After subsequent molecular dynamics (MD) simulation taking into account the explicit lipid membrane molecules with periodic boundary conditions, we obtained multiple model structures of the GPCRs. For each target structure, docking–screening calculations were carried out via the ensemble docking procedure, using both true active compounds of the target proteins and the UAPs with the multiple target screening (MTS) method. Consequently, the multiple model structures showed various screening results with both poor and high hit ratios, the latter of which could be identified as promising for use in in silico screening to find candidate compounds to interact with the proteins. We found that the hit ratio of true active compounds showed a positive correlation to that of the UAPs. Thus, we could retrieve appropriate target structures from the GPCR models by applying the UAPs, even if no active compound is known for the GPCRs. Namely, the screening result that showed a high hit ratio for the UAPs could be used to identify actual hit compounds for the target GPCRs.



## 1. INTRODUCTION

G-protein coupled receptors (GPCRs) are important target molecules in pharmaceutical science. To perform structure-based in silico drug screening, the three-dimensional (3D) structure of a target protein must be known. Unfortunately, 3D structures are available only for a  $\beta_1$ -adrenergic receptor (ADRB1),  $\beta_2$ -adrenergic receptor (ADRB2),  $A_{2A}$  adenosine receptor ( $A_{2A}$ ), and dopamine D3 receptor ( $D_3$ ), C–X–C chemokine receptor type 4, and rhodopsin. Thus, in most cases, the 3D structures of GPCRs must be created from these known structures by homology modeling.

In general, structure-based drug screening based on the homology model has provided poor results. There have been many reports about the relationship between target modeling methods and hit ratios.<sup>1–5</sup> Some reports have suggested that the hit ratios depend on structural changes in the ligand-binding pockets.<sup>2,3</sup> McGovern et al.<sup>1</sup> have reported that the holo crystal structures would provide better enrichment than the apo crystal structures and that the apo structures would provide better enrichment than the homology modeled structures. We reported

that the model structures obtained by the molecular dynamics (MD) simulations would provide poorer enrichment than the crystal structures.<sup>6</sup> However, the number of examples was small, and a more comprehensive study is needed to better understand how to prepare the most suitable 3D structure model for the target protein.<sup>7</sup>

Even if target protein structures determined by X-ray crystallography experiments are used, in silico screening succeeds in providing good database enrichment in approximately half of the cases, and it fails in hit compound prediction in the other half of the cases.<sup>8</sup> In addition, even a slight structural change around the binding site will sometimes have a large effect on the docking scores.<sup>2,3</sup>

Ensemble docking is becoming a trend in the structure-based in silico drug screening.<sup>9–12</sup> In the ensemble docking, multiple target protein structures are prepared in order to consider the flexibility of the protein structure. The compounds in the library

**Received:** May 25, 2011

**Published:** August 17, 2011

are docked to these multiple structures. If some active compounds are known for their target proteins, then a structure that shows good hit ratios of these known active compounds should be selected as a suitable protein structure for the docking screening study. The ensemble docking is effective in some cases, but one problem is how to select a target structure that will give good screening results among multiple protein structures. If no active compound is known for the target protein, then it is difficult to select a suitable protein structure for the docking screening study.

In a previous study, we prepared a set of drug-like compounds called universal active probes (UAPs) and performed *in silico* drug screening based on an ensemble docking study.<sup>12</sup> The hit ratio of the true active compounds was proportional to that of the UAPs. Thus, a structure that gives the best UAP hit ratio should give a good hit ratio in drug screening even if no active compound is known.

In the present study, we focused on the ensemble docking of GPCRs. We examined the application of an ensemble of 3D structures generated by the MD simulation from a homology model. We then applied the UAPs to select a structure from the ensemble. We identified the UAPs that were useful among several types of UAPs, and we assessed the usefulness of this protocol.

## 2. METHODS

**2.1. Preparation of GPCR Structures.** We first studied three GPCRs, ADRB2, A<sub>2A</sub>, and D<sub>3</sub>, whose 3D crystal structures are known and their PDB IDs are 2rh1, 3eml, and 3pbl, respectively. Then, by conventional homology modeling procedures, we prepared the 3D structures of the other nine GPCRs whose 3D structures were unknown ( $\beta_1$ -adrenergic receptor, ADRB1 (exception, 3D structure is known);  $\beta_3$ -adrenergic receptor, ADRB3; histamine H<sub>2</sub> receptor, H<sub>2</sub>; histamine H<sub>3</sub> receptor, H<sub>3</sub>; dopamine D<sub>2</sub> receptor, D<sub>2</sub>; 5-hydroxytryptamine receptor 1A, 5-HT<sub>1A</sub>; 5-hydroxytryptamine receptor 2A, 5-HT<sub>2A</sub>; muscarinic acetylcholine receptor M<sub>1</sub>, M<sub>1</sub>; and  $\mu$  opioid receptor: MOR).

Multiple amino acid sequence alignments were performed by MAFFTash,<sup>13,14</sup> and the alignments were edited manually to align the conserved amino acids. The multiple alignment results are summarized in the Supporting Information. The initial 3D coordinates were generated by the MODELER homology modeling program,<sup>15,16</sup> using four template structures, ADRB2 (PDBID: 2rh1) for ADRB3; 5HT-1A, 5HT-2A, H<sub>2</sub>, H<sub>3</sub>, MOR, and A<sub>2A</sub> (3eml) for M<sub>1</sub>; D<sub>3</sub> (3pbl) for D<sub>2</sub>; and turkey ADRB1 (2vt4) for human ADRB1. We generated up to three energetically preferable candidate structures as initial models using MODELER. The crystal structures of ADRB2 and A<sub>2A</sub> include the fused lysozyme, which was removed from the GPCR parts for the current study. The N- and C-terminals were capped by acetyl and N-methyl groups, respectively.

The following MD simulation generated multiple structures starting from the three crystal structures and from  $9 \times 3$  model structures generated by the homology modeling. The MD simulations were performed in an explicit membrane and water system. The charges of protein atoms and the force field were originated from AMBER parm99.<sup>17</sup> The systems were solvated in a box of ca. 83 Å (horizontal direction to the membrane)  $\times$  83 Å (horizontal direction to the membrane)  $\times$  102 Å (perpendicular direction to the membrane). The whole structure of each protein

was embedded in POPE lipid bilayers and TIP3P<sup>18</sup> water including ion particles of Cl<sup>-</sup> in order to neutralize the total charge of the systems. Periodic boundary conditions were applied, and Berendsen's algorithm<sup>19</sup> for temperature and pressure coupling was adopted (300 K and 1 atm, respectively). After a first steepest descent (1000 steps) and conjugated gradient (1000 steps) energy minimizations with positional restraints on the solute, an initial 100 ps simulation was carried out with the positions of the solute atoms restrained by a force constant of 10 kcal/(mol Å<sup>2</sup>) to let the water diffuse around the molecule and for equilibration. The particle mesh Ewald method (PME)<sup>20</sup> was used to calculate the electrostatic contribution to nonbonded interactions with a cutoff of 12 Å and a time step of 1 fs. The cutoff distance of the van der Waals interaction was 12.0 Å. After this equilibration run, the NVT production run (1 ns) at 300 K was performed with the cell size remaining the same. The SHAKE algorithm was applied to the system, and the time step was set to 2 fs.<sup>21</sup> The MD simulations were performed by using cosgene/myPresto.<sup>22</sup> Snapshot structures were obtained at every 50 ps as the target structures extracted from a trajectory of 1 ns. In addition, the initial and energy-minimized structures were used in the following study. Finally, we obtained one energy-minimized structure and 20 snapshot structures for each initial structure that was given as the crystal structure or by the homology modeling procedure. Cosgene/myPresto is available at [http://presto.protein.osaka-u.ac.jp/myPresto4/index\\_e.html](http://presto.protein.osaka-u.ac.jp/myPresto4/index_e.html).

**2.2. Preparation of Chemical Compounds.** The compound library consisted of 540 known ligands for 12 target proteins and a decoy set. The numbers of known agonists were 54, 42, 17, 17, 17, 19, 17, 20, 7, 20, 12, and 11 for 5-HT<sub>1A</sub>, 5-HT<sub>2A</sub>, A<sub>2A</sub>, ADRB1, ADRB2, ADRB3, D<sub>2</sub>, D<sub>3</sub>, H<sub>2</sub>, H<sub>3</sub>, M<sub>1</sub>, and MOR, respectively. The numbers of known antagonists were 34, 50, 17, 24, 18, 11, 38, 38, 21, 27, 14, 11 for 5-HT<sub>1A</sub>, 5-HT<sub>2A</sub>, A<sub>2A</sub>, ADRB1, ADRB2, ADRB3, D<sub>2</sub>, H<sub>2</sub>, H<sub>3</sub>, M<sub>1</sub>, and MOR, respectively. The SMILES representation of each known ligand is summarized in the Supporting Information.

The decoy set (decoy 1) consists of 11 013 compounds of the Coelacanth chemical compound library (Coelacanth Chemical Corporation, East Windsor, NJ), which is a random library. The other decoy (decoy 2) set consists of 10 000 randomly selected compounds from the LiganBox database.<sup>23</sup>

The 3D coordinates of 11 013 chemical compounds of decoy set 1 were generated by the Concord program (Tripos, St. Louis, MO) from the 2D Sybyl SD files provided by Coelacanth Chemical Corporation. The atomic charges of each compound in decoy set 1 were determined by the Gasteiger method.<sup>24,25</sup> How to generate the 3D coordinates and how to calculate the atomic charges of the compounds of decoy 2 were described in detail elsewhere.<sup>23</sup> The 3D coordinates were generated by the cosgene (conformer search engine) MD simulation program<sup>22</sup> with the general AMBER force field (GAFF),<sup>26</sup> and the atomic charges were calculated by the MOPAC AM1 method [Quantum Chemistry Program Exchange (QCPE), Indiana University, Bloomington, IN].

The 3D coordinates of the known ligands were generated by the Chem3D program (Cambridge Software, Cambridge, MA). The atomic charges of each known ligand were determined by the Gasteiger method. The docking results obtained by the sievgen docking program do not depend on the atomic charges so much.<sup>31</sup>

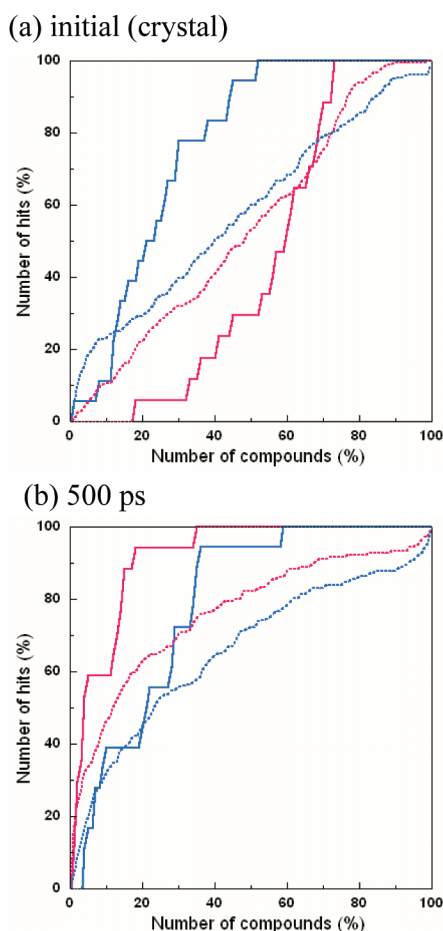


**Figure 1.** Database enrichment curves for (a) the initial crystal structure of ADRB2 (2rh1) and (b) the snapshot structure at 500 ps of ADRB2 on the MD run 1. The solid red and blue and dotted red and blue lines represent the results obtained for the true agonists, true antagonists, UAP\_GPCR1, and UAP\_GPCR2, respectively.

**2.3. Screening Method and Protein Set.** The structure-based *in silico* drug screening was performed by using the SievGene protein–compound docking program.<sup>27</sup> For flexible docking, up to 100 conformers were generated for each ligand. The multiple target screening (MTS) method was used as the *in silico* drug screening method in the present study.<sup>28,29</sup> The basic idea of the MTS method is that a potential active compound is that which shows the strongest affinity to the target protein among many proteins. Such compounds are then sorted according to the docking scores. Thus, based on the multiple protein–multiple compound docking score panel (affinity matrix), the compounds that show the strongest affinities to the target proteins are selected as hit compounds. We therefore must prepare a set of proteins including target proteins. For each target structure, an individual protein set was prepared. Each protein set consisted of a basic protein set and the target structure itself. The protein set consists of 181 proteins listed in Appendix A (basic protein set), which were also used in our previous study.<sup>29</sup> To perform the docking simulation, the SievGene/myPresto protein–compound docking program was used.<sup>27</sup> The docking program, the MTS screening tools, and the 3D structures of the proteins used are available at [http://presto.protein.osaka-u.ac.jp/myPresto4/index\\_e.html](http://presto.protein.osaka-u.ac.jp/myPresto4/index_e.html).

The preparation procedure for the target proteins is described in Section 2.1. They were the same ones used to evaluate the docking programs, GOLD and FlexX,<sup>30</sup> and they were also used in our previous works to evaluate our *in silico* screening program.<sup>12,28,29,31,32</sup> The data set contains a rich variety of proteins and compounds whose structures were all determined by high-quality experiments with a resolution of less than 2.5 Å. Almost all of the atom coordinates are supplied, except for those of the hydrogen atoms, and the all-atomic structures around the ligand pockets are quite reliable. None of the complex structures had any covalent interactions between the proteins and the ligands. The docking program, the MTS screening tools, and the 3D structures of the proteins used are available at [http://presto.protein.osaka-u.ac.jp/myPresto4/index\\_e.html](http://presto.protein.osaka-u.ac.jp/myPresto4/index_e.html).

### 3. RESULTS AND DISCUSSION

**3.1. Ensemble Docking for MD Structures from the Antagonist-Bound GPCR Conformations.** We first made an ordinary ensemble docking study by preparing many different structures for each of the three antagonist-bound GPCRs, ADRB2, A<sub>2A</sub>, and D<sub>3</sub>, by MD simulation with explicit solvent and lipid membrane molecules. Three independent 1 ns MD simulations were performed for each GPCR system, with a different initial atom velocity applied in each simulation. No antagonists or agonists were included during any of the MD simulations. Figures S1 and S2, Supporting Information show the trajectories of the root-mean-square deviation (RMSD) of heavy atoms around the active sites. The RMSDs of the active site atoms of ADRB2 snapshot structures from the initial crystal structure with the antagonist were in the range of 1.5–2.0 Å, and they are plotted in Figure S1a, Supporting Information. Figure 1 shows examples of database enrichment curves of the snapshot structures with the MTS screening method for the antagonists and agonists (blue and red solid lines, respectively). The areas under those database enrichment curves (AUC) are plotted in Figure 2a, b, and c for the three GPCR structures extracted from the MD simulations at every 50 ps, in addition to their initial crystal structures and the successive energy-minimized structures. Table 1 summarizes the maximum, minimum, and average AUC values and the corresponding hit ratios at 1% compounds selected for the three GPCRs. The AUC values with the other decoy set 2 are shown in Figure S3a, b, and c, Supporting Information.

It is clear that for both decoys, appropriate GPCR structures appeared with AUC values high enough for drug screening of both the antagonists and agonists, although the initial MD structure was the crystal structure of an antagonist-bound form. Significantly low AUC values sometimes appeared for several structures, whose active site volumes are too small or too large, probably because the MD simulation did not include any ligand molecules at their active sites and because large numbers of different snapshot structures were sampled. For ADRB2, the RMSDs of the active site atoms from the recent agonist-bound structure (PDB ID: 3p0g) were also in the range of 1.5–2.0 Å, as shown in Figure S1b, Supporting Information. Although the RMSD values from the agonist-bound form are slightly larger than those from the antagonist-bound form, the two active site structures are similar. Consequently, high AUC values for the agonists were obtained even in the structural ensembles starting from the antagonist-bound forms. This may be because the interaction energy potential between the ligand and the receptor



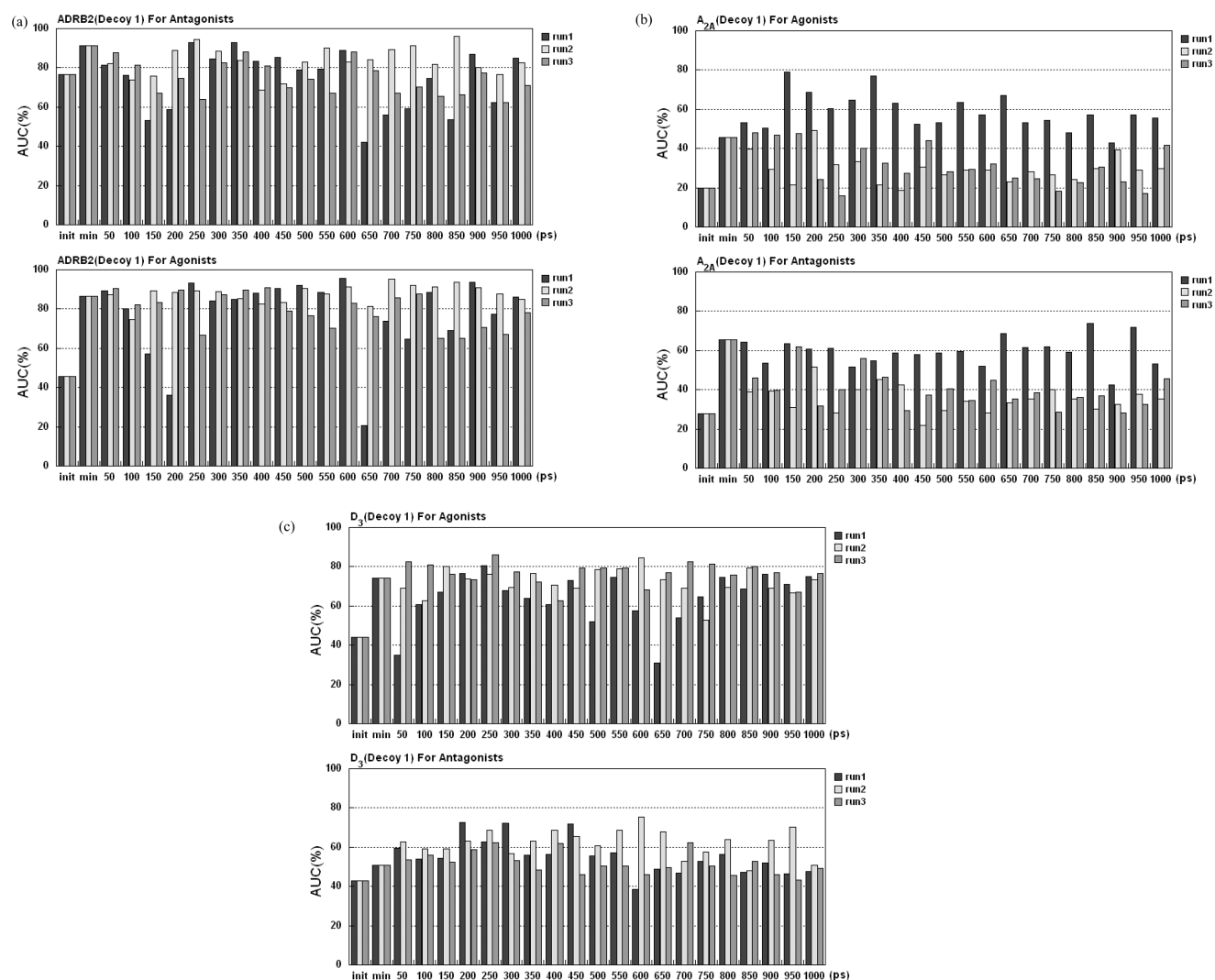


Figure 2. The AUC values for the agonists and antagonists of ADRB2 (a), A<sub>2A</sub> (b), and D<sub>3</sub> (c) receptors with decoy set 1.

Table 1. Maximum, Minimum, and Average AUC Values with the Corresponding Hit Ratios at 1% Compounds for the Snapshot Structures of Three GPCRs: ADRB2, A<sub>2A</sub>, and D<sub>3</sub><sup>a</sup>

		AUC max	AUC min	AUC average	Hit ratio max	Hit ratio min	Hit ratio average
(a) Decoy Set 1							
ADRB2	antagonists	96.0	42.0	77.7 ± 11.5	33.3	0.0	7.5 ± 8.7
	agonists	95.6	57.0	80.2 ± 14.9	70.6	0.0	18.1 ± 20.0
A <sub>2A</sub>	antagonists	73.7	21.9	45.0 ± 13.6	11.8	0.0	0.4 ± 1.8
	agonists	78.9	15.9	39.2 ± 16.1	0.0	0.0	0.0 ± 0.0
D <sub>3</sub>	antagonists	75.5	38.6	55.7 ± 8.6	10.5	0.0	2.2 ± 2.6
	agonists	86.0	30.8	70.0 ± 11.6	20.0	0.0	7.0 ± 6.4
(b) Decoy Set 2							
ADRB2	antagonists	84.3	29.6	54.8 ± 12.2	11.1	0.0	1.2 ± 2.5
	agonists	76.4	29.8	61.0 ± 11.0	23.5	0.0	2.1 ± 4.8
A <sub>2A</sub>	antagonists	61.5	27.0	41.9 ± 7.7	5.9	0.0	0.4 ± 1.4
	agonists	70.6	16.6	42.6 ± 11.6	5.9	0.0	0.1 ± 0.7
D <sub>3</sub>	antagonists	67.6	18.6	36.7 ± 12.7	5.3	0.0	0.4 ± 1.1
	agonists	74.3	27.4	48.9 ± 9.3	10.0	0.0	1.1 ± 2.4

<sup>a</sup> A random screening and an ideal screening give that AUC = 50 and 100, respectively.

**Table 2.** Maximum, Minimum, And Average AUC Values with the Corresponding Hit Ratios at 1% Compounds for the Snapshot Structures of the Nine Modeled GPCRs<sup>a</sup>

		AUC max	AUC min	AUC average	hit ratio maximum	hit ratio minimum	hit ratio average
(a) Decoy Set 1							
ADRB1	antagonists	79.6	35.7	57.5 ± 10.6	29.2	0.0	3.0 ± 5.1
	agonists	92.2	31.5	67.3 ± 17.9	29.4	0.0	9.1 ± 10.6
ADRB3	antagonists	83.6	26.3	62.6 ± 13.9	18.2	0.0	2.5 ± 4.9
	agonists	75.3	35.8	56.2 ± 9.7	15.8	0.0	2.7 ± 4.4
H <sub>2</sub>	antagonists	90.5	17.4	61.3 ± 18.7	26.8	0.0	7.8 ± 6.6
	agonists	98.6	2.9	63.5 ± 24.1	57.1	0.0	10.6 ± 11.8
H <sub>3</sub>	antagonists	76.5	15.5	47.4 ± 13.3	22.0	0.0	2.6 ± 3.7
	agonists	95.8	1.8	57.1 ± 27.0	80.0	0.0	19.9 ± 25.3
D <sub>2</sub>	antagonists	72.7	43.9	59.6 ± 6.7	13.2	0.0	2.4 ± 3.2
	agonists	88.5	30.1	66.1 ± 11.3	23.5	0.0	2.5 ± 4.5
5-HT <sub>1A</sub>	antagonists	75.8	36.9	58.1 ± 9.7	14.7	0.0	2.9 ± 4.0
	agonists	77.9	34.3	59.2 ± 11.6	20.4	0.0	3.9 ± 4.7
5-HT <sub>2A</sub>	antagonists	74.0	38.7	58.5 ± 7.1	8.0	0.0	2.1 ± 2.0
	agonists	86.0	43.4	70.0 ± 9.9	42.9	0.0	11.3 ± 12.9
M <sub>1</sub>	antagonists	85.4	36.9	56.9 ± 10.4	14.3	0.0	1.9 ± 3.7
	agonists	97.0	24.5	65.2 ± 19.6	75.0	0.0	11.5 ± 17.7
MOR	antagonists	93.7	4.5	64.1 ± 22.9	36.4	0.0	6.9 ± 10.9
	agonists	93.4	14.2	67.2 ± 18.4	45.5	0.0	10.2 ± 12.2
(b) Decoy Set 2							
ADRB1	antagonists	71.2	21.6	45.2 ± 13.6	12.5	0.0	1.3 ± 2.7
	agonists	69.4	30.9	51.4 ± 9.0	17.6	0.0	2.0 ± 3.8
ADRB3	antagonists	76.7	18.6	45.8 ± 10.8	9.1	0.0	0.4 ± 1.9
	agonists	65.4	24.7	42.6 ± 10.7	10.5	0.0	0.9 ± 2.2
H <sub>2</sub>	antagonists	73.2	22.7	49.2 ± 11.3	14.3	0.0	3.0 ± 4.3
	agonists	88.1	21.6	50.9 ± 14.7	28.6	0.0	3.0 ± 6.4
H <sub>3</sub>	antagonists	83.9	17.9	53.1 ± 14.8	14.8	0.0	2.5 ± 4.1
	agonists	87.7	11.0	54.9 ± 20.9	65.0	0.0	9.8 ± 14.7
D <sub>2</sub>	antagonists	77.3	26.8	47.7 ± 11.0	7.9	0.0	1.5 ± 2.2
	agonists	68.1	28.1	52.4 ± 8.7	11.8	0.0	0.8 ± 2.3
5-HT <sub>1A</sub>	antagonists	75.8	36.9	58.1 ± 9.7	14.7	0.0	2.2 ± 3.3
	agonists	77.9	34.3	59.2 ± 11.6	5.6	0.0	1.5 ± 1.8
5-HT <sub>2A</sub>	antagonists	79.5	22.6	43.3 ± 13.5	10.0	0.0	1.0 ± 1.9
	agonists	69.3	37.7	56.1 ± 7.7	28.6	0.0	4.3 ± 5.7
M <sub>1</sub>	antagonists	73.9	23.6	52.9 ± 12.4	7.1	0.0	0.9 ± 2.3
	agonists	85.5	20.5	59.6 ± 13.2	33.3	0.0	4.3 ± 6.6
MOR	antagonists	93.1	4.5	44.0 ± 18.9	54.5	0.0	1.8 ± 7.3
	agonists	83.8	5.3	48.2 ± 19.4	36.4	0.0	4.0 ± 7.3

<sup>a</sup> A random screening and an ideal screening give that AUC = 50 and 100, respectively.

is designed to be soft enough to cover minor differences in our docking program, SievGene.

**3.2. Ensemble Docking for Agonists and Antagonists with the Homology Models.** Homology models were constructed for nine GPCRs, human ADRB1, human ADRB3, H<sub>2</sub>, H<sub>3</sub>, D<sub>2</sub>, 5-HT<sub>1A</sub>, 5-HT<sub>2A</sub>, M<sub>1</sub>, and MOR, from the antagonist-bound crystal structures of their closest homologues, as indicated in the Methods Section. Starting from three different homology models for each GPCR, 1 ns MD simulations with explicit solvent and membrane molecules were performed to prepare their structural ensemble. As shown in Figure S2, Supporting Information, the RMSDs of the active site atoms of the human ADRB1 snapshots deviated by about 2 Å from the agonist-bound crystal structure

(PDB ID: 2y02) during the MD simulation. Although the initial structures for the MD simulations were constructed by homology modeling based on the turkey ADRB1 antagonist-bound crystal structure, these deviations were only slightly larger than those for the snapshot structures starting from the actual crystal structures, shown in Figure S1a and b, Supporting Information. This suggests that the quality of our homology models for the human ADRB1 was high enough for the ensemble docking study, as was also the case in Section 3.1.

Screening calculations were performed for the structural ensembles. Table 2 summarizes the maximum, minimum, and average AUC values for the snapshot structures with the corresponding hit ratios at 1% compounds with decoy sets 1 and 2.

Table 3. Distributions of Properties of Compound Sets

		decoy set 1	decoy set 2	agonist UAP_GPCR1	antagonist UAP_GPCR2	UAP_DUD	UAP_PDB
number of rings	average	4.2	2.8	2.8	3.4	3.0	2.2
	SD <sup>a</sup>	1.1	0.9	1.2	1.3	1.0	1.8
molecular weight (Da)	average	423.4	316.7	304.5	369.5	304.6	367.0
	SD <sup>a</sup>	63.6	43.1	96.9	73.4	29.0	184.9
number of heavy atoms	average	30.9	22.3	21.6	26.2	21.6	25.8
	SD <sup>a</sup>	4.7	3.3	6.9	5.2	2.4	13.3

<sup>a</sup>SD is the standard deviation.

The AUC values of the snapshot structures for both the antagonists and the agonists with decoy set 1 are shown in Figure S3a–i, Supporting Information. The AUC values with decoy set 2 are shown in Figure S4a–i, Supporting Information.

Again, appropriate structural models for screening appeared with sufficiently high AUC values in all cases, although there are sometimes few structures having high AUC values, in particular H3 antagonists with decoy set 1 and ADRB1, ADRB3, and D<sub>2</sub> with decoy set 2. For decoy set 1, 3.5 and 17.0% of the structures showed AUC values >90 and >80% for antagonist screening, while 17.0% of the structures showed very low (<50%) AUC values for antagonist screening. For agonist screening, 1.0 and 6.2% of the structures showed AUC values >90 and >80%, while 24.4% of the structures showed very low (<50%) AUC values. For decoy set 2, 0.0 and 2.7% of the structures showed AUC values >90 and >80% for antagonist screening, while 45.3% of the structures showed very low (<50%) AUC values. For agonist screening, 0.2 and 0.3% of the structures showed AUC values >90 and >80%, while 50.0% structures showed very low (50%) AUC values.

These results suggest that our modeling procedure succeeded in generating GPCR structures that could be used for drug screening, although the population of GPCR structures that gave high hit ratios was low.

For most of the GPCRs, high AUC values were observed for decoy set 2 as well as for decoy set 1, although the AUC values for decoy set 2 were generally lower than those for decoy set 1. This may suggest the molecular feature of the decoy set (sets 1 and 2) is different from that of the GPCR ligands (see Table 3).

In many cases, the AUC values of the MD snapshot structures were higher than those of the initial structures, suggesting that the relaxed structures may be better for screening than the initial structure based on the template structure, which binds particular antagonists. Also, starting from the same initial structure, the AUC value changed drastically at every 50 ps. This suggests that the AUC value strongly depends on changes in the structure. This is consistent with the previous reports,<sup>8,33</sup> showing that in silico drug screening by structure-based screening methods depended strongly on the 3D structure of the target protein. Generally speaking, in silico screening succeeds in providing good database enrichment in approximately half of the cases, and it fails in hit compound prediction in the other half. In some cases, the prediction results are much worse than the results obtained by random screening. In addition, even a slight structural change around the binding site could sometimes have a large effect on the docking scores.<sup>2,3</sup> Therefore, success in ensemble docking depends on the number and quality of the structures prepared in the ensemble, which should cover many different and possible 3D receptor conformations, covering even the structural change upon binding of both the antagonists and

agonists. The current ensemble docking procedure could generate GPCR model structures effective for in silico docking of both the antagonists and agonists, although the model structures were constructed based on the antagonist-bound template structures.

**3.3. How To Select a GPCR Structure if Known Ligands Are Not Available.** If known ligands are available, we can select a candidate protein structure that shows a good in silico screening result, or we can apply the machine-learning multiple target screening (MS-MTS) method to the target.<sup>29</sup> The problem is how to select a suitable protein structure among many structures for in silico screening in the absence of any known active compounds. Previously, we introduced the idea of an UAP.<sup>12</sup> The UAP is a drug-like compound. In that study, the UAPs were ligands of proteins from protein–ligand complex structures registered in the PDB, active compounds selected from the directory of useful decoys (DUD)<sup>34</sup> and ligands of the GPCRs. For soluble proteins, the hit ratio of true active compounds was proportional to that of the UAPs in ensemble docking. In the current study, we applied the UAP to the GPCRs.

In the present study, we adopted the UAP selected from the DUD (UAP\_DUD) and that selected from the PDB (UAP\_PDB); these UAPs were exactly the same as those used in the previous study.<sup>12</sup> In addition, we prepared UAP\_GPCR1 and UAP\_GPCR2 sets. UAP\_GPCR1 and UAP\_GPCR2 sets consisted of all of the agonists and all of the antagonists used in the present study, respectively. The distributions of the number of rings, mass weight, and number of heavy atoms are summarized in Table 3. The size distributions of the compound sets used were qualitatively similar to each other. The agonists were smaller than the antagonists. The distributions of decoy sets mostly overlapped with those of GPCR ligands, while decoy set 1 was slightly larger than the other sets.

The database enrichment curve was calculated for the true active compounds, and the AUC<sub>true</sub> was calculated as a measure of the screening result. Also, the database enrichment curve was calculated for the UAPs, and the AUC<sub>UAP</sub> was also calculated. In Figure 1, two examples of database enrichment curves are shown for the ADRB2 initial crystal structure and the snapshot structures at 500 ps. When the hit ratio of the UAP\_GPCR2 is higher than that of the UAP\_GPCR1, the hit ratio of the antagonist is higher than that of the agonist and vice versa. The database enrichment curves for the snapshot structures at initial and 500 ps using the UAPs indicate that the selected structures are effective enough to be applied as well as those selected by the true active compounds.

Finally, the AUC<sub>true</sub> and AUC<sub>UAP</sub> values were compared, and the correlation coefficient between the AUC<sub>true</sub> value and the AUC<sub>UAP</sub> value for all MD snapshots of a given target was calculated. This scheme is exactly the same as that in our previous

Table 4. Correlation Coefficients (*R*) between AUC<sub>true</sub> and AUC<sub>UAP</sub> Values (decoy set 1)

target		UAP_GPCR1	UAP_GPCR2	UAP_DUD	UAP_PDB
ADRB1	agonist	0.925	0.651	0.883	0.848
	antagonist	0.658	0.707	0.595	0.509
ADRB2	agonist	0.864	0.486	0.857	0.87
	antagonist	0.582	0.462	0.683	0.365
ADRB3	agonist	0.709	0.796	0.677	0.498
	antagonist	0.739	0.669	0.728	0.621
H <sub>2</sub>	agonist	0.867	0.829	0.831	0.762
	antagonist	0.867	0.905	0.843	0.751
H <sub>3</sub>	agonist	0.847	0.597	0.744	0.927
	antagonist	0.664	0.793	0.606	0.463
D <sub>2</sub>	agonist	0.839	0.733	0.849	0.776
	antagonist	0.737	0.734	0.695	0.554
D <sub>3</sub>	agonist	0.906	0.806	0.940	0.85
	antagonist	0.803	0.919	0.733	0.643
5-HT <sub>1A</sub>	agonist	0.801	0.911	0.740	0.662
	antagonist	0.658	0.801	0.552	0.605
5-HT <sub>2A</sub>	agonist	0.931	0.676	0.907	0.874
	antagonist	0.628	0.825	0.448	0.400
M <sub>1</sub>	agonist	0.910	0.748	0.777	0.832
	antagonist	0.713	0.596	0.657	0.629
MOR	agonist	0.654	0.603	0.548	0.705
	antagonist	0.696	0.601	0.702	0.705
A <sub>2A</sub>	agonist	0.892	0.879	0.811	0.850
	antagonist	0.888	0.879	0.909	0.811
averaged <i>R</i> for all ligands		0.741	0.723	0.684	0.644
averaged <i>R</i> for agonists		0.849	0.771	0.787	0.796
averaged <i>R</i> for antagonists		0.608	0.728	0.508	0.503

study.<sup>11</sup> For UAP\_GPCR1 and UAP\_GPCR2, the true agonists or antagonists of the target GPCR were removed from the analysis.

The correlation coefficients are summarized in Tables 4 and 5 for decoy sets 1 and 2, respectively. All the correlation coefficients were positive in Table 4. In Table 5, most of the correlation coefficients were positive except for those of UAP\_DUD. In general, the AUC<sub>true</sub> value is positively correlated with the AUC<sub>UAP</sub> value, as are the previous results for soluble proteins. The correlation between the AUC<sub>true</sub> and the AUC of UAP\_GPCR was stronger than the other correlations.

The average correlation coefficients between UAP\_GPCR2 and the GPCR antagonist were 0.728 and 0.629 for decoy sets 1 and 2, respectively; these values were as high as those of the soluble protein cases reported in our previous study.<sup>12</sup> In addition, the average correlation coefficient between UAP\_GPCR2 and the GPCR agonist was only 0.179 for decoy set 2. Thus, UAP\_GPCR2 was useful for selecting the antagonist screening result. The UAP\_GPCR1 was also useful for selecting the agonist screening result, since the average correlation coefficients between UAP\_GPCR1 and the GPCR agonist were 0.849 and 0.312 for decoy sets 1 and 2, respectively. The value for decoy set 2 was lower than that for decoy set 1. This trend is not very clear, since the deviation of the correlation coefficients was 0.2–0.6, which was almost equivalent to the difference between the correlation coefficients of agonists and antagonists.

The UAP\_PDB was also useful for selecting the GPCR ligand screening, but we could not distinguish the screening results for antagonists from those for agonists, as is shown in Tables 4 and 5.

On the contrary, the UAP\_DUD was not useful. The average correlation coefficient for decoy set 1 was positive, but that for decoy set 2 was negative. As shown in Table 3, the number of rings, molecular weight, and number of heavy atoms of the UAP\_GPCR1 are almost equal to those of the UAP\_DUD. This result shows that the shape of the compound is as important as the UAP.

When the structures that showed the best hit ratios of the UPAs were selected, the average AUC value and the average hit ratio at 1% compounds selected are summarized in Table 6. The agonist and antagonist screenings were done by using UAP\_GPCR1 and UAP\_GPCR2, respectively. For UAP\_GPCR1 and UAP\_GPCR2, the true agonists or antagonists of the target GPCR were removed. Although the AUC<sub>UAP</sub> values for the best structures selected by UPAs are always lower than those for the best structures selected by the AUC<sub>true</sub>, as shown in Table 2, their AUC<sub>UAP</sub> values and the hit ratios are significantly higher than the average values for all of the corresponding structural ensemble, as shown in Table 6. In fact, by using the UAP, the AUC<sub>UAP</sub> values and the hit ratios were improved by 1.1–1.3 and 1.2–2.1 times, respectively, from those obtained by all generated structures in the ensemble.

Our previous study showed that the UAP protocol worked for the soluble proteins whose 3D coordinates were experimentally determined.<sup>12</sup> The present study showed that the UAP protocol worked for the modeled GPCR structures. We are now applying the UAP protocol to a homology-modeled soluble protein. In near future, the domain of applicability of the UAP will be clear.

Table 5. Correlation Coefficients (*R*) between AUC<sub>true</sub> and AUC<sub>UAP</sub> Values (decoy set 2)

target		UAP_GPCR1	UAP_GPCR2	UAP_DUD	UAP_PDB
ADRB1	agonist	0.011	−0.387	−0.308	−0.098
	antagonist	0.525	0.788	−0.371	0.481
ADRB2	agonist	0.365	−0.341	0.043	0.412
	antagonist	0.152	0.452	−0.236	−0.312
ADRB3	agonist	0.266	0.826	−0.255	0.243
	antagonist	0.288	0.437	−0.200	0.273
H <sub>2</sub>	agonist	0.175	0.158	−0.166	−0.277
	antagonist	−0.026	0.538	−0.384	−0.245
H <sub>3</sub>	agonist	0.460	−0.346	0.107	0.270
	antagonist	0.315	0.865	−0.529	0.400
D <sub>2</sub>	agonist	0.315	0.341	0.206	0.235
	antagonist	0.290	0.746	0.142	0.232
D <sub>3</sub>	agonist	0.056	0.037	−0.006	0.083
	antagonist	0.244	0.236	0.174	0.213
5-HT <sub>1A</sub>	agonist	0.108	0.861	−0.482	0.448
	antagonist	0.161	0.937	−0.542	0.625
5-HT <sub>2A</sub>	agonist	0.722	0.227	0.184	0.549
	antagonist	0.469	0.923	−0.355	0.063
M <sub>1</sub>	agonist	0.477	−0.289	−0.239	−0.092
	antagonist	0.256	0.614	−0.133	0.581
MOR	agonist	0.373	0.633	−0.307	0.491
	antagonist	0.241	0.384	−0.069	0.324
A <sub>2A</sub>	agonist	0.412	0.431	−0.391	0.323
	antagonist	0.182	0.140	0.355	0.259
averaged <i>R</i> for all ligands		0.298	0.421	−0.147	0.248
averaged <i>R</i> for agonists		0.312	0.179	−0.135	0.216
averaged <i>R</i> for antagonists		0.286	0.629	−0.158	0.276

Table 6. Averaged AUC Values and Averaged Hit Ratios at 1% Compounds for the 9 GPCRs

		decoy set 1		decoy set 2	
		averaged overall structures	selected by UAP	averaged overall structures	selected by UAP
agonist	AUC (%)	63.4	77.6	51.5	58.6
	hit ratio	8.9	12.6	2.8	5.3
antagonist	AUC (%)	58.7	70.0	47.0	62.9
	hit ratio	3.5	4.1	1.4	3.0

We used the MD-MVO method to calculate the similarity between compound sets.<sup>35</sup> The MD-MVO method calculates the volume overlap between two compounds considering their atomic charges. One hundred compounds each were randomly selected from UAP\_GPCR1, UAP\_GPCR2, UAP\_DUD, UAP\_PDB, and decoy sets 1 and 2, so that a total of 600 compounds were selected. The similarities among these 600 compounds (= 600 \* 600) were calculated by the MD-MVO method. The similarity scores were averaged in each group and the results are summarized in Tables S1–S3, Supporting Information. The similarity between compounds in UAP\_GPCR1 and UAP\_GPCR2 was not much greater than their similarities to the other sets. As a result, it could be concluded that UAP\_GPCR worked not because the GPCR ligands were similar to each other but because of something else.

#### 4. CONCLUSION

We applied the ensemble docking study to 12 GPCRs. The structural ensembles of the GPCRs were generated by MD simulations starting from the antagonist-bound form or by homology models with successive MD simulations in explicit solvent and membrane environments. The screening results depended strongly on the slight structural changes in the GPCRs due to the structural flexibility and adjustability of the protein. The UAPs were applied to the selection of the most effective structure from the GPCR structural ensemble generated by the MD simulation. Since the hit ratio of the UAPs was proportional to that of the true active compounds, the structures that showed high hit ratios of true active compounds could be selected by using the UAP concept. Our ensemble docking procedure with the UAP was successfully performed



for both antagonist and agonist screening, although the average screening results without selection by the UAP were lower than the results with selection.

## APPENDIX A

The protein databank (PDB) identifier list of the basic protein set is: 1a28, 1a42, 1a4g, 1a4q, 1abe1, 1abe2, 1abf1, 1abf2, 1aco, 1ai5, 1aoe, 1apt, 1apu, 1aqw, 1atl, 1b58, 1b9v, 1bma, 1byb, 1byg, 1c1e, 1c5c, 1c83, 1cbs, 1cbx, 1cdg, 1ckp, 1com, 1coy, 1cps, 1cvu, 1d0l, 1d3h, 1dd7, 1dg5, 1dhf, 1dog, 1dr1, 1ebg, 1eed, 1ejn, 1epb, 1epo, 1ets, 1f0r, 1f0s, 1f3d, 1fen, 1fkg, 1fki, 1fl3, 1glp, 1hdc, 1hfc, 1hos, 1hqv, 1hsb, 1hsl, 1htf1, 1htf2, 1hyt, 1ida, 1liv, 1jap, 1lah, 1lcp, 1lic, 1lna, 1lst, 1mdr, 1mld, 1mmq, 1mrg, 1mts, 1mup, 1nco, 1ngp, 1nis, 1okl, 1pbd, 1phd, 1phg, 1poc, 1ppc, 1pph, 1pso, 1qbr, 1qbu, 1qqp, 1rds, 1rne, 1rnt, 1rob, 1snc, 1srj, 1tlp, 1tmn, 1tng, 1tnh, 1tni, 1tnl, 1tyl, 1xid, 1xie, 1yee, 2aad, 2ack, 2ada, 2cht, 2cmd, 2cpp, 2ctc, 2fox, 2gbp, 2ifb, 2pk4, 2qwk, 2tmn, 3cla, 3cpa, 3erd, 3ert, 3tpi, 4lbd, 4phv, 5abp1, 5abp2, 5cpp, 5er1, 6rnt, and 7tim. For 1abe, 1abf, 5abp, and 1htf, two protein pockets were prepared, since these proteins each bind two kinds of ligands.

## ASSOCIATED CONTENT

**S Supporting Information.** The UAP\_GPCR1 and UAP\_GPCR2 are available in the SMILES format. The AUC values for 12 GPCRs for decoy set 2 are also available. This material is available free of charge via the Internet at <http://pubs.acs.org>.

## AUTHOR INFORMATION

### Corresponding Author

\*E-mail: y-fukunishi@aist.go.jp. Telephone: +81-3-3599-8290.

## ACKNOWLEDGMENT

This work was supported by grants from the New Energy and Industrial Technology Development Organization of Japan (NEDO) and from the Ministry of Economy, Trade, and Industry (METI) of Japan.

## REFERENCES

- (1) McGovern, S. L.; Shoichet, B. K. Information decay in molecular docking screens against holo, apo, and modeled conformations of enzymes. *J. Med. Chem.* **2003**, *46*, 2895–2907.
- (2) Oshiro, C.; Bradley, E. K.; Eksterowicz, J.; Evensen, E.; Lamb, M. L.; Lancot, K.; Putta, S.; Stanton, R.; Grootenhuis, D. J. Performance of 3D-database molecular docking studies into homology models. *J. Med. Chem.* **2004**, *47*, 764–767.
- (3) DeWesse-Scott, C.; Moulton, J. Molecular modeling of protein function regions. *Proteins* **2004**, *55*, 942–961.
- (4) Diller, D. J.; Li, R. Kinases, homology models, and high throughput docking. *J. Med. Chem.* **2003**, *46*, 4638–4647.
- (5) Bissantz, C.; Bernard, P.; Hibert, M.; Rognan, D. Protein-based virtual screening of chemical databases. II. Are homology models of G-Protein Coupled Receptors suitable targets? *Proteins* **2003**, *50*, 5–25.
- (6) Omagari, K.; Mitomo, D.; Kubota, S.; Nakamura, H.; Fukunishi, Y. A method to enhance the hit ratio by a combination of structure-based drug screening and ligand-based screening. *Adv. Appl. Bioinf. Chem.* **2008**, *1*, 19–28.
- (7) Lerner, M. G.; Bowman, A. L.; Carlson, H. A. Incorporating dynamics in E. coli dihydrofolate reductase enhances structure-based drug discovery. *J. Chem. Inf. Model.* **2007**, *47*, 2358–2365.
- (8) Warren, G. L.; Webster Andrews, C.; Capelli, A. M.; Clarke, B.; LaLonde, J.; Lambert, M. H.; Lindvall, M.; Nevins, N.; Semus, S. F.; Senger, S.; Tedesco, G.; Wall, I. D.; Woolven, J. M.; Peishoff, C. E.; Head, M. S. A Critical Assessment of Docking Programs and Scoring Functions. *J. Med. Chem.* **2006**, *49*, 5912–5931.
- (9) Rueda, M.; Bottegoni, G.; Abagyan, R. Recipes for the selection of experimental protein conformations for virtual screening. *J. Chem. Inf. Model.* **2010**, *50*, 186–193.
- (10) Barakat, K.; Mane, J.; Friesen, D.; Tuszyński, J. Ensemble-based virtual screening reveals dual-inhibitors for the p53-MDM2/MDMX interactions. *J. Mol. Graphics Modell.* **2010**, *28*, 555–568.
- (11) Craig, I. R.; Essex, J.; Spiegel, K. Ensemble docking into multiple crystallographically derived protein structures: an evaluation based on the statistical analysis of enrichment. *J. Chem. Inf. Model.* **2010**, *50*, 511–524.
- (12) Fukunishi, Y.; Ono, K.; Orita, M.; Nakamura, H. Selection of in silico drug screening result by using universal active probes (UAPs). *J. Chem. Inf. Model.* **2010**, *50*, 1233–1240.
- (13) Standley, D. M.; Toh, H.; Nakamura, H. ASH structure alignment package: sensitivity and selectivity in domain classification. *BMC Bioinformatics* **2007**, *8*, 116.
- (14) Katoh, K.; Misawa, K.; Kuma, K.; Miyata, T. MAFFT: a novel method for rapid multiple sequence alignment based on fast Fourier transform. *Nucleic Acids Res.* **2002**, *30*, 3059–3066.
- (15) Sali, A.; Blundell, T. L. Comparative protein modelling by satisfaction of spatial restraints. *J. Mol. Biol.* **1993**, *234*, 779–815.
- (16) Marti-Renom, M. A.; Stuart, A.; Fiser, A.; Sánchez, R.; Melo, F.; Sali, A. Comparative protein structure modeling of genes and genomes. *Annu. Rev. Biophys. Biomol. Struct.* **2000**, *29*, 291–325.
- (17) Case, D. A.; Darden, T. A.; Cheatham, T. E., III; Simmerling, C. L.; Wang, J.; Duke, R. E.; Luo, R.; Merz, K. M.; Wang, B.; Pearlman, D. A.; Crowley, M.; Brozell, S.; Tsui, V.; Gohlke, H.; Mongan, J.; Hornak, V.; Cui, G.; Beroza, P.; Schafmeister, C.; Caldwell, J. W.; Ross, W. S.; Kollman, P. A. AMBER 8; University of California: San Francisco, CA, 2004.
- (18) Jorgensen, W. L.; Chandrasekhar, J.; Madura, J. D.; Impey, R. W.; Klein, M. L. Comparison of simple potential functions for simulating lipid water. *J. Chem. Phys.* **1983**, *79*, 926–935.
- (19) Berendsen, H. J. C.; Postma, J. P. M.; van Gunsteren, W. F.; DiNola, A.; Haak, J. R. Molecular dynamics with coupling to an external bath. *J. Chem. Phys.* **1984**, *81*, 3684–3690.
- (20) Darden, T.; York, D.; Pedersen, L. Particle mesh Ewald: an N-log(N) method for Ewald sums in large systems. *J. Chem. Phys.* **1993**, *98*, 10089–10092.
- (21) Ryckaert, J. P.; Ciccotti, G.; Berendsen, H. J. C. Numerical integration of the cartesian equations of motion of a system with constraints: Molecular dynamics of n-alkanes. *J. Comput. Phys.* **1997**, *23*, 327–341.
- (22) Fukunishi, Y.; Mikami, Y.; Nakamura, H. The filling potential method: A method for estimating the free energy surface for protein-ligand docking. *J. Phys. Chem. B* **2003**, *107*, 13201–13210.
- (23) Fukunishi, Y.; Sugihara, Y.; Mikami, Y.; Sakai, K.; Kusudo, H.; Nakamura, H. Advanced in silico drug screening to achieve high hit ratio-development of 3D-compound database. *Synthesiology* **2009**, *2*, 60–68.
- (24) Gasteiger, J.; Marsili, M. Iterative partial equalization of orbital electronegativity — a rapid access to atomic charges. *Tetrahedron* **1980**, *36*, 3219–3228.
- (25) Gasteiger, J.; Marsili, M. A new model for calculating atomic charges in molecules. *Tetrahedron Lett.* **1978**, 3181–3184.
- (26) Wang, J.; Wolf, R. M.; Caldwell, J. W.; Kollman, P. A.; Case, D. A. Development and testing of a general amber force field. *J. Comput. Chem.* **2004**, *25*, 1157–1174.
- (27) Fukunishi, Y.; Mikami, Y.; Nakamura, H. Similarities among receptor pockets and among compounds: Analysis and application to in silico ligand screening. *J. Mol. Graphics Modell.* **2005**, *24*, 34–45.
- (28) Fukunishi, Y.; Mikami, Y.; Kubota, S.; Nakamura, H. Multiple target screening method for robust and accurate in silico ligand screening. *J. Mol. Graphics Modell.* **2005**, *25*, 61–70.

- (29) Fukunishi, Y.; Kubota, S.; Nakamura, H. Noise reduction method for molecular interaction energy: application to in silico drug screening and in silico target protein screening. *J. Chem. Inf. Model.* **2006**, *46*, 2071–2084.
- (30) Nissink, J. W. M.; Murray, C.; Hartshorn, M.; Verdonk, M. L.; Cole, J. C.; Taylor, R. A new test set for validating predictions of protein-ligand interaction. *Proteins* **2002**, *49*, 457–471.
- (31) Fukunishi, Y.; Mashimo, T.; Orita, M.; Ohno, K.; Nakamura, H. In silico fragment screening by replica generation (FSRG) method for fragment-based drug design. *J. Chem. Inf. Model.* **2009**, *49*, 925–933.
- (32) Fukunishi, Y.; Nakamura, H. Improvement of protein-compound docking scores by using amino-acid sequence similarities of proteins. *J. Chem. Inf. Model.* **2008**, *48*, 148–156.
- (33) Kontoyianni, M.; Sokol, G. S.; McClellan, L. M. Evaluation of library ranking efficacy in virtual screening. *J. Comput. Chem.* **2005**, *26*, 11–22.
- (34) Huang, N.; Shoichet, B. K.; Irwin, J. J. Benchmarking sets for molecular docking. *J. Med. Chem.* **2006**, *49*, 6789–6801.
- (35) Fukunishi, Y.; Nakamura, H. A new method for in silico drug screening and similarity search using molecular-dynamics maximum-volume overlap (MD-MVO) method. *J. Mol. Graphics Modell.* **2009**, *27*, 628–636.